

# 3D Measurement of Transparent Vessel and Submerged Object Using Laser Range Finder

Hirotoishi Ibe

Graduate School of Science and  
Technology, Shizuoka University  
3-5-1 Johoku, Naka-ku, Hamamatsu-shi,  
Shizuoka 432-8561, Japan

Atsushi Yamashita

Department of Precision  
Engineering, The University of Tokyo  
7-3-1 Hongo, Bunkyo-ku, Tokyo  
113-8656, Japan

Toru Kaneko

and Yuichi Kobayashi  
Department of Mechanical  
Engineering, Shizuoka University  
3-5-1 Johoku, Naka-ku, Hamamatsu-shi,  
Shizuoka 432-8561, Japan

**Abstract**—Specimens of precious underwater creatures are preserved in transparent vessels with liquid. It is important to measure three-dimensional shape of submerged objects. When measuring submerged objects by image measurement, refraction of light should be considered. This problem can be solved by ray tracing, but the 3D coordinates of the vessel are necessary.

In this paper, we propose a method of measuring both a vessel and an object by using a laser range finder (LRF) mounted on a manipulator. Because a transparent vessel is not completely transparent, a reflection from the vessel surface can be detected in addition to a reflection from the object. However, the captured image may have many reflections from various paths, then it is necessary to detect correct reflections. The proposed method solves this problem by examining a behavior of each reflection relating to the epipolar constraint when the posture of the LRF is changed.

Experimental results show the effectiveness of the proposed method.

**Index Terms**—Underwater Image Measurement, Laser Range Finder, 3D-Measurement, Epipolar Constraint.

## I. INTRODUCTION

Recently, digital archives of important objects (e.g. cultural assets or prehistoric site) are created by various measurement technology [1]. Although many objects are in the air, some objects are kept in liquid. For example, specimens of precious underwater creatures, such as abyssal fish, are preserved in transparent vessels filled with liquid. Creation of digital archives of submerged objects requires a measurement method in liquid environment without damaging objects.

Ultrasonic measurement techniques find wide use in underwater sensing. However, to measure submerged objects in a vessel is difficult because of multi echoes.

Image measurement methods can acquire position and color of measured object by using captured image. Those techniques are measurable at short distance, because attenuation of light through a liquid. 3D measurement methods of liquid environment (mainly underwater) have been proposed [2][3][4][5]. In this paper, to measure submerged object in transparent vessel we employ image measurement.

To measure submerged object by image measurement, it is necessary to consider effects of refraction of light. A light from a submerged object to a camera passes through a liquid, a vessel (e.g. glass or acryl) and air. The refractive indices of those media differ. Therefore, the outside surface and the

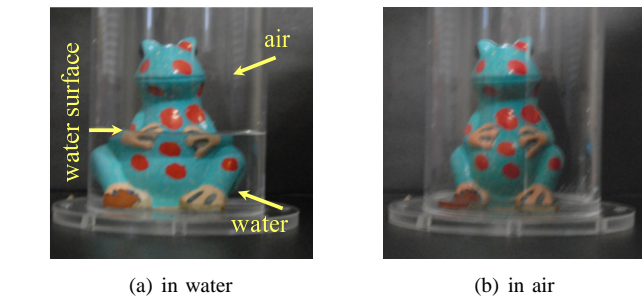


Fig. 1. Refraction effect.

inside surface of the vessel become refraction surfaces at which the direction of light is changed. The outside surface is a boundary of air and the vessel. The inside surface is a boundary of vessel and the liquid. An example of refraction effect is shown in Fig. 1. Fig. 1(a) is an image of a frog model in a vessel which is half filled with water, and Fig. 1(b) is an image without water. The appearances of those images under water surface differ by refraction of light. When a captured image is distorted by refraction, we cannot obtain accuracy in measurement.

Li et al. proposed a method to measure submerged object by ray tracing to consider refraction of light [2]. This method determines the geometry of refraction boundary by using a calibration pattern. After calibration, this method measures submerged objects. When we use this method in order to measure an object in a vessel, shape and position of transparent surfaces (outside and inside surface of vessel) are required.

Ikeda et al. proposed a method for 3D measurement of both a transparent vessel and a submerged object by using Laser Range Finder (LRF) which consists of a beam light laser and a camera mounted on a manipulator [4]. The measurement model of this approach is shown in Fig. 2. A part of irradiated light from the laser of LRF is reflected at the outside surface of the transparent vessel (this reflected light is hereinafter called as vessel reflection in this paper), and the majority of irradiated light penetrates the transparent vessel. The penetrated light is reflected at the submerged object (this reflected light is hereinafter called as object reflection in this paper). Both vessel reflection and object reflection are

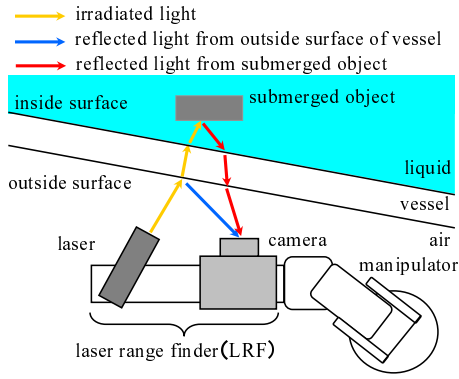


Fig. 2. Measurement model.

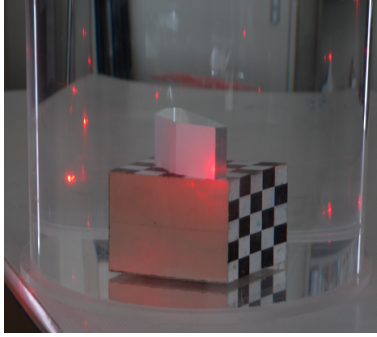


Fig. 3. Reflected lights through various paths.

captured with the camera of LRF. In general, vessel reflection is very weak but detectable because a transparent vessel is not completely transparent. Therefore, both the transparent vessel and the submerged object can be measured by triangulation using reflections in captured images.

The above method assumes that a captured image contain only vessel reflection and object reflection. However, reflections from various paths may exist in the image (Fig. 3). Then, this method makes a measurement error when a false reflection is chosen for triangulation.

In this paper, we propose a method for 3D measurement of a submerged object in a transparent vessel of unknown shape by using the LRF. The method chooses the correct reflection in the image for triangulation by examining the behavior of the reflection made by posture change of the LRF. Then, it determines the 3D coordinates of the vessel surface, and obtains the shape of the object by ray tracing.

## II. OUTLINE

The proposed method performs 3D measurement of the vessel and the submerged object by using the LRF mounted on the manipulator. The LRF, moving along the vessel surface, irradiates a laser beam onto the object through the vessel and captures an image of laser spots reflected at both the vessel surface and the object surface.

The schematic diagram of the proposed method is the same as shown in Fig.2. A light beam emitted from the laser source

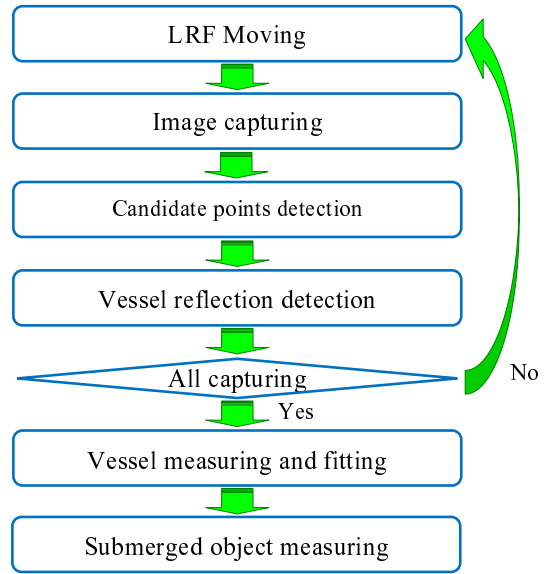


Fig. 4. Procedure flow.

is projected into the vessel. The beam is partly reflected at the vessel surface in the direction to the camera. The remaining light beam penetrates the vessel, refracted twice on the outside and the inside of the vessel surfaces, and reaches to the object. The light reflected at the object again reaches to the camera after the refraction on the inside and the outside of the vessel surface. The proposed method captures the image of reflections both at the vessel surface and the object surface, and measures the shapes of the vessel and the object.

The procedure flow is shown in Fig. 4. First, the LRF is moved to a measurement position. Then, an image is captured with the camera. In the image, candidates for reflections from the vessel and the object are detected. Among the candidates, the reflection from the vessel is identified. These steps are repeated until it is executed for all the measurement positions. After acquisition of the all data of the reflections, the method calculates the 3D coordinates of the vessel surface by triangulation, and executes model fitting. Finally, the shape of the submerged object is obtained by ray tracing.

Fig.5 shows an example of movement of measurement position.

## III. PRINCIPLE OF MEASUREMENT

### A. Detection of candidate points

The following describes a process to detect candidate points for vessel reflections and object reflections in a captured image with the camera.

A method proposed in [4] employs image thresholding to detect candidate points. However, this technique is not appropriate, because the intensity of the vessel reflection is very unstable. Then, we employ a peak filter to detect candidate points, assuming that those points have local peak intensities in the image. The procedure of detection is shown in Fig. 6.

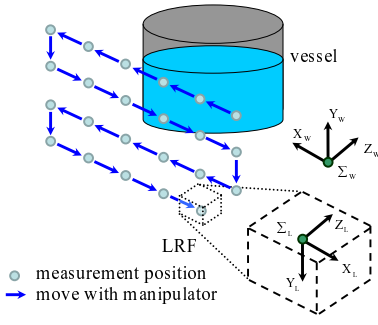


Fig. 5. Image capturing with zigzag scanning.

Captured images with the camera have RGB color information. A weighted averaging converts an RGB color image to a grayscale image which has intensity information by considering the color property of the laser. Prior to peak filtering, a noise of the converted grayscale image is decreased by smoothing. We employ Gaussian smoothing.

The peak filter converts a grayscale image to a peak image which consists of peak pixel (1) and no peak pixel (0), as shown in the following.

$$P(u, v) = \begin{cases} 1 & \text{if } I(u, v) = I_{max}(u, v), \psi(u, v) = 1 \\ 0 & \text{otherwise} \end{cases} \quad (1)$$

where  $P(u, v)$  is a value of the peak image at attention pixel  $(u, v)$  whose intensity is  $I(u, v)$ ,  $I_{max}(u, v)$  is the maximum intensity of peripheral pixels of  $(u, v)$ , and  $\psi(u, v)$  is a factor to reduce the effect of noise in low intensities.

$$\psi(u, v) = \begin{cases} 1 & \text{if } I_{max}(u, v) - I_{min}(u, v) > T_p \\ 0 & \text{otherwise} \end{cases} \quad (2)$$

where  $I_{min}(u, v)$  is the minimum intensity of peripheral pixels and  $T_p$  is a threshold.

This filter determines a pixel as the peak pixel when its intensity is equal to the local maximum. All pixels in the captured image are executed this operations.

It is possible that one peak pixel spreads to several pixels by saturation. Therefore, labeling is executed to concatenate peak pixels to one group in an image. We acquire the candidate points to calculate the center of the gravity of concatenated groups.

### B. Detection of vessel reflection

To acquire a position of vessel reflection, we propose a method of identification with changing a posture of the LRF and a method of reflection tracking. Fig. 7 shows the procedure of identification and tracking of vessel reflection.

A vessel reflection satisfies the epipolar constraint. Therefore, a position  $(u_d, v_d)$  of the vessel reflection is restricted in the vicinity of the epipolar line with error tolerance  $T_e$  as follows.

$$|v_d - (a_e u_d + b_e)| < T_e. \quad (3)$$

where  $a_e$  and  $b_e$  are parameters representing the epipolar line.

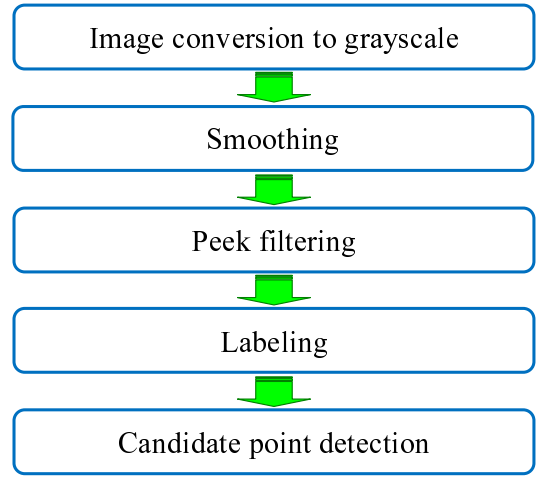


Fig. 6. Detection of candidate points.

When two or more candidate points exist along the epipolar line, it is necessary to choose the vessel reflection among the candidate points. If we change the posture of the LRF, those candidate points move in the image (Fig. 8). The movement of the vessel reflection is restricted on the epipolar line. On the other hand, false candidate points may leave from the epipolar line. Accordingly, false candidate points can be removed with (3) by changing the posture of the LRF with the manipulator gradually. This process continues until a single candidate point is determined as the vessel reflection.

Here, it is not efficient to identify vessel reflections by the above process frequently. The vessel reflection can be tracked from image to image because positions of laser irradiation on the vessel between two consecutive measurements are close to each other, if we assume the movement is very small and the surface of the vessel is smooth. Then, once the vessel reflection is identified in a measurement, we track the vessel reflection in the image of next measurement efficiently. However, the vessel reflection cannot be tracked when close points to the previous vessel reflection exist.

Hence, we combine identification and tracking approaches. When a previous vessel reflection exists and tracking works, the tracked point is the vessel reflection. If tracking does not work, identification process is executed.

### C. Measurement of transparent vessel and model fitting

Measurement of the vessel surface by triangulation begins with the measurement of the outside surface using the outside reflection points. From the 3D coordinates of measured point group, the method fits an approximating geometric model to the group. Then the method determines the normal vectors on the outside vessel surface from the approximated model, and estimates the 3D coordinates of points at the inside vessel surface by assuming that the thickness of the vessel is uniform. The approximating geometric model of the inside vessel surface is also determined.

In the above triangulation, accuracy of the image coordi-

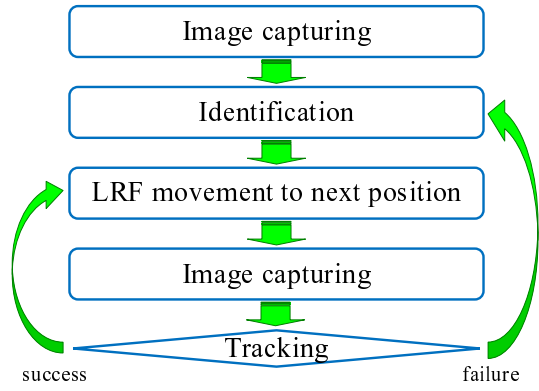


Fig. 7. Detection of vessel reflection.

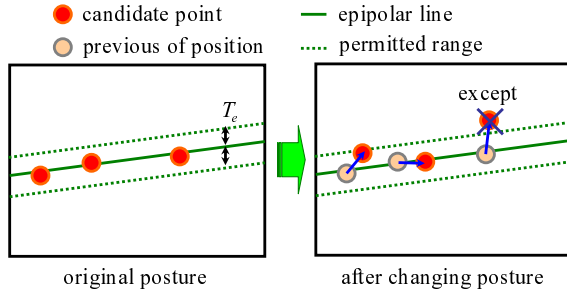


Fig. 8. Vessel reflection identifying with changing posture.

ates of the vessel reflection is very important. However, there are some deviations between reflections and the epipolar line, because of noise. Then, we project the image coordinate of the reflection peak onto the epipolar line in the image, and execute correction in sub-pixel order by interpolating the peak position of approximated Gaussian distribution estimated by the intensity profile on the epipolar line [6].

#### D. Measurement of submerged object

Measurement of the submerged object is realized by ray tracing [2] of the laser from the LRF and the camera image. Fig. 9 shows the geometry of ray tracing of the laser. This ray starts in the direction of  $\mathbf{v}_{l1} = (\alpha_1, \beta_1, \gamma_1)^T$  from position  $\mathbf{p}_{l1}$  which is the position of laser light source. Symbols  $n_1$ ,  $n_2$  and  $n_3$  are refractive indices of air, vessel and liquid.

The position  $\mathbf{p}_{l2}$  and the normal vector  $\mathbf{m}_1 = (\lambda_1, \mu_1, \nu_1)^T$  at the intersection of the outside surface of the vessel are obtained by using the approximating model of the vessel surface. The direction vector  $\mathbf{v}_{l2} = (\alpha_2, \beta_2, \gamma_2)^T$  of the ray in the vessel is calculated based on Snell's law as follows.

$$\begin{pmatrix} \alpha_2 \\ \beta_2 \\ \gamma_2 \end{pmatrix} = \frac{n_1}{n_2} \begin{pmatrix} \alpha_1 \\ \beta_1 \\ \gamma_1 \end{pmatrix} + \kappa_1 \begin{pmatrix} \lambda_1 \\ \mu_1 \\ \nu_1 \end{pmatrix}, \quad (4)$$

where

$$\kappa_1 = \left[ \sqrt{1 - (1 - t_1^2) \left( \frac{n_1}{n_2} \right)^2} - t_1 \left( \frac{n_1}{n_2} \right) \right], \quad (5)$$

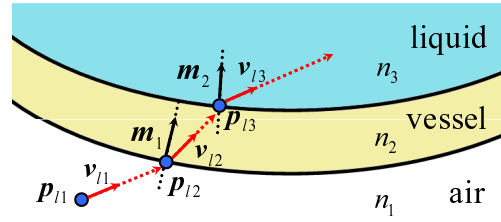


Fig. 9. Ray tracing.

$$t_1 = (\mathbf{v}_{l1} \cdot \mathbf{m}_1). \quad (6)$$

The position  $\mathbf{p}_{l3}$  and the normal vector  $\mathbf{m}_2 = (\lambda_2, \mu_2, \nu_2)^T$  at the intersection of the inside surface of the vessel are also determined by using the approximated model. The direction vector  $\mathbf{v}_{l3} = (\alpha_3, \beta_3, \gamma_3)^T$  of the ray in the vessel is also calculated.

$$\begin{pmatrix} \alpha_3 \\ \beta_3 \\ \gamma_3 \end{pmatrix} = \frac{n_2}{n_3} \begin{pmatrix} \alpha_2 \\ \beta_2 \\ \gamma_2 \end{pmatrix} + \kappa_2 \begin{pmatrix} \lambda_2 \\ \mu_2 \\ \nu_2 \end{pmatrix}, \quad (7)$$

where

$$\kappa_2 = \left[ \sqrt{1 - (1 - t_2^2) \left( \frac{n_2}{n_3} \right)^2} - t_2 \left( \frac{n_2}{n_3} \right) \right], \quad (8)$$

$$t_2 = (\mathbf{v}_{l2} \cdot \mathbf{m}_2). \quad (9)$$

These direction and normal vectors  $\mathbf{v}_{l1}$ ,  $\mathbf{v}_{l2}$ ,  $\mathbf{v}_{l3}$ ,  $\mathbf{m}_1$  and  $\mathbf{m}_2$  are all unit vectors. Similarly, the ray of the camera is calculated by ray tracing.

The intersection of the rays of the laser and the camera is determined as the 3D measurement point of the object. Generally, the two rays do not have an intersection because of noises, then the mid point of two rays which are nearest to each other is determined as the measurement point.

Measurement of submerged object needs detection of correct reflection of the object in the image. If there are multiple candidate points in the image, a candidate point whose ray and the laser ray has a distance longer than a threshold is removed as a false reflection. Among the remaining candidate points, the candidate points that has the maximum intensity is determined as the object reflection.

## IV. EXPERIMENTS

Fig. 10 shows the measurement system used for experiments. The manipulator had three axes for changing posture to identify vessel reflections. Posture changing was executed by unit of 1 degree in the range of  $\pm 10$  degrees. Specifications of the system are shown in Table I. The experiments were executed in a darkroom.

TABLE I  
SPECIFICATIONS OF THE SYSTEM

Camera resolution	1024 × 768 pixel
Wavelength of laser	635 nm (red color)
Manipulator movement	1 mm

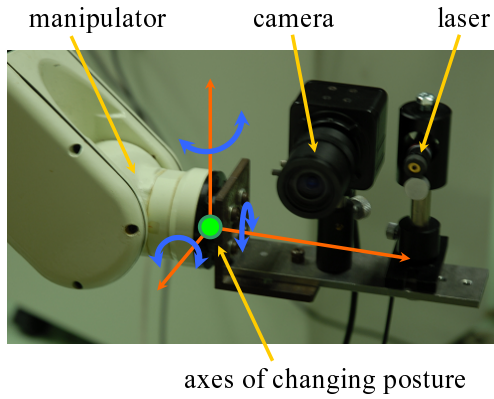


Fig. 10. Measurement system.



Fig. 11. Glass vessel.

#### A. Ascertainment of vessel reflection detection

A glass vessel (Fig. 11) was measured to ascertain a performance of vessel reflection detection.

Table II shows a result. In many cases, vessel reflections were detected by tracking. In rare cases, detection was failed because the intensity of vessel reflection was too weak to capture with the camera. An example of detection process is shown in Fig. 12. A captured image in original posture (Fig. 12(a)) has 3 candidate points along the epipolar line. In the second posture (Fig. 12(b)), the candidate point at right side was excepted because it disappeared. In the third posture (Fig. 12(c)), the candidate point at left side was excepted because it moved off the epipolar line. Hence, the middle point was identified as the vessel reflection (Fig. 12(d)).

A measurement result of the glass vessel is shown in Fig. 13. Fig. 13(a) is the result by our proposed method, and Fig. 13(b) is the result by a simple method. The result by a simple method has errors derived from detection of false reflections. On the other hand, the result of our method shows the correct shape of the glass vessel.

TABLE II  
DETAIL OF VESSEL REFLECTION DETECTION

Measurement position	100 × 40 (4000) points
Frequency of identification process	27
Frequency of tracking process	3934
Frequency of detection failure	39

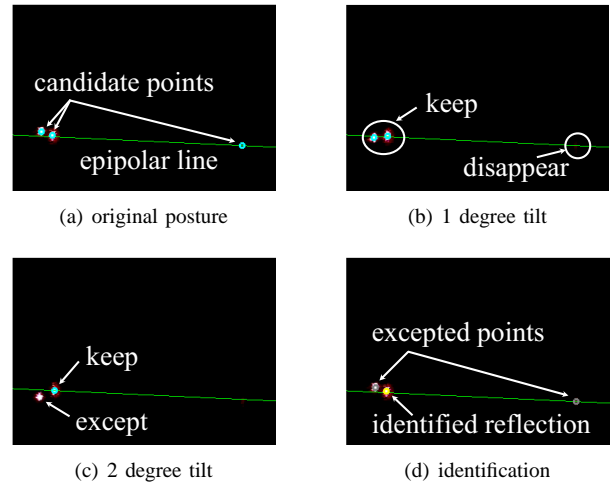


Fig. 12. Process of vessel reflection identification.

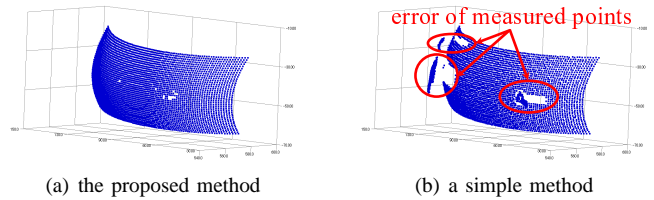


Fig. 13. Measurement of glass vessel.

#### B. Evaluation of measurement accuracy

The accuracy of our system was evaluated by measuring a trapezoid object in a cylindrical vessel filled with water. The cylindrical vessel is shown in Fig. 14 and the trapezoid object is shown in Fig. 15. Our system measured the planes (the middle, right and left) of the trapezoid object. The width of the middle plane (50 mm) and the angles of the middle plane between both side planes (30 deg.) were evaluated. Table III details the conditions of the measurement.

Fig. 16 shows a measurement result of outside surface of the vessel in the coordinate system of the cylinder. The radius of the outside surface was estimated as 165.5 mm from this result by using the Nelder-Mead method [7].

The measurement result of the trapezoid object based on ray tracing through the estimated cylindrical model is shown in Fig. 17. It is shown in Fig. 18 that measured points are divided into three planes and there are two crossing lines of planes. The width of the middle plane was calculated as the distance between the crossing lines. In addition, the angle between the crossing lines was calculated to evaluate the parallelism.

Those evaluation results are shown in Table IV. As the result, the accuracy of our measurement system was confirmed. The scale error was within 1 mm and the angle error was within 1 degree.

#### C. Measurement of submerged object

A submerged object which is a model of dolphin in Fig. 19 was measured instead of specimens. In this experiment, the



Fig. 14. Cylindrical vessel.

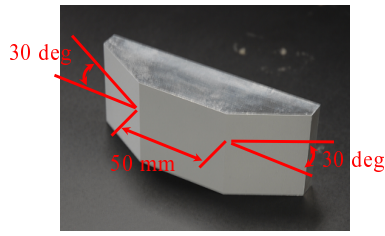


Fig. 15. Trapezoid object.

TABLE III  
DETAIL OF MEASUREMENT FOR ACCURACY TEST

Measurement position	250 × 40 (10000) points
Radius of cylindrical vessel	165.5 mm
Thickness of cylindrical vessel	5 mm
Material of cylindrical vessel	acryl
Width of trapezoid object	50 mm
Angles of trapezoid object	30 degree
Refractive index	air:1.00, acryl:1.49, water:1.33

same vessel and liquid in Table III was used. The number of measurement positions is 250 × 70 (17500 points).

Fig. 20 shows measured points of the submerged object. As the result, the shape of the dolphin is expressed in detail.

## V. CONCLUSION

We propose a method for 3D measurement of a transparent vessel and submerged objects by using the LRF mounted on a manipulator. The method makes it possible to measure objects in a transparent vessel of unknown shape. Experimental results show the effectiveness of the proposed method.

As a future work, the 3D shape of a submerged object should be created by combining measurement results obtained from multiple viewpoints.

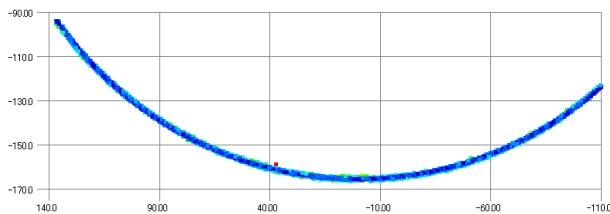


Fig. 16. Measurement result of cylindrical vessel.

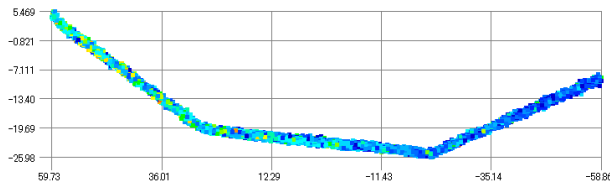


Fig. 17. Measurement result of trapezoid object.

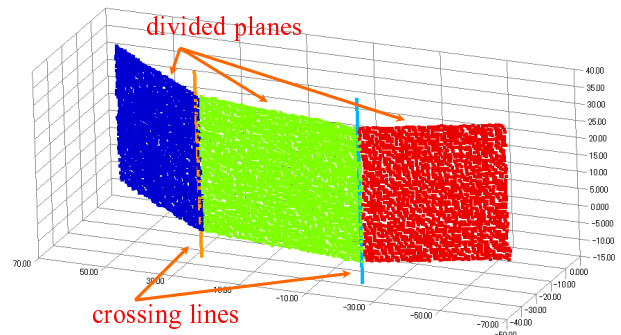


Fig. 18. Evaluation of measurement result.

TABLE IV  
EVALUATION RESULT OF TRAPEZOID PLANE

	Measured value	Ground truth
Distance of crossing lines [mm]	49.5	50.0
Angle of crossing lines [deg.]	0.4	0.0
Angle of middle - right [deg.]	29.8	30.0
Angle of middle - left [deg.]	30.5	30.0

## REFERENCES

- [1] Y. Okamoto, T. Oishi and K. Ikeuchi, "Image-Based Network Rendering of Large Meshes for Cloud Computing," *International Journal of Computer Vision*, Vol.94, Issue 1, pp.12-22, August 2011.
- [2] R. Li, H. Li, W. Zou, R. G. Smith and T. A. Curran, "Quantitative Photogrammetric Analysis of Digital Underwater Video Imagery," *IEEE Journal of Oceanic Engineering*, 22(2):364-375, April 1997.
- [3] A. K. Chong and P. Stanford, "Underwater Digital Stereo-Observation Technique for Red Hydrocoral Study," *Photogrammetric Engineering and Remote Sensing*, Vol.68, No.7, pp.745-751, July 2002.
- [4] A. Yamashita, S. Ikeda and T. Kaneko, "3-D Measurement of Objects in Unknown Aquatic Environments with a Laser Range Finder," in *Proceedings of the 2005 IEEE International Conference on Robotics and Automation*, pp.3923-3928, April 2005.
- [5] A. Yamashita, R. Kawanishi, T. Koketsu, T. Kaneko and H. Asama, "Underwater Sensing with Omni-Directional Stereo Camera," in *Proceedings of the 2011 IEEE International Conference on Computer Vision Workshop (OMNIVIS2011)*, pp.304-311, November 2011.
- [6] A. Prokos, G. Karras and E. Petsa, "Automatic 3D Surface Reconstruction by Combining Stereovision with the Slit-Scanner Approach," in *Proceedings of the International Archives of Photogrammetry, Remote Sensing and Spatial Information Sciences (ISPRS)*, Vol. XXXVIII, Part 5, pp.505-509, June 2010.
- [7] J. A. Nelder and R. Mead, "A Simplex Method for Function Minimization," *Computer Journal*, Vol.7, pp.308-313, 1965.



Fig. 19. Model of dolphin.

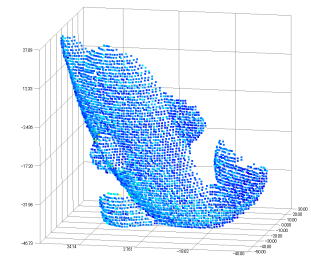


Fig. 20. Measurement result.